Determination of the atmospheric lifetime and global warming potential of sulphur hexafluoride using a three-dimensional model

Tamás Kovács[1], Wuhu Feng[1,2], Anna Totterdill[1], John M.C. Plane[1], Sandip Dhomse[2], Juan Carlos Gómez-Martín[1], Gabriele P. Stiller[3], Florian J. Haenel[3], Christopher Smith[4], Piers M. Forster[2], Rolando R. García[5], Daniel R. Marsh[5] and Martyn P. Chipperfield[2]*

[1]School of Chemistry, University of Leeds, Leeds LS2 9JT, UK.
[2]NCAS, School of Earth and Environment, University of Leeds, Leeds LS2 9JT, UK.
[3]Karlsruhe Institute of Technology, IMK-ASF, PO BOX 3640, 76021 Karlsruhe, Germany.
[4]Energy Research Institute, School of Chemical and Process Engineering, University of Leeds, Leeds LS2 9JT, UK.
[5]National Center for Atmospheric Research (NCAR), Boulder, Colorado, USA.

Correspondence to: Martyn Chipperfield (M.Chipperfield@leeds.ac.uk)

Abstract. We have used the Whole Atmosphere Community Climate Model (WACCM), with an updated treatment of loss processes, to determine the atmospheric lifetime of SF_6. The model includes the following SF_6 removal processes: photolysis, electron attachment and reaction with mesospheric metal atoms. The Sodankylä Ion Chemistry (SIC) model is incorporated into the standard version of WACCM to produce a new version with a detailed *D* region ion chemistry with cluster ions and negative ions. This is used to determine a latitude- and altitude-dependent scaling factor for the electron density in the standard WACCM in order to carry out multi-year SF_6 simulations. The model gives a mean SF_6 lifetime over a 11-year solar cycle (τ) of 1278 years (with a range from 1120 to 1475 years), which is much shorter than the currently widely used value of 3200 years, due to the larger contribution (97.4%) of the modelled electron density to the total atmospheric loss. The loss of SF_6 by reaction with mesospheric metal atoms (Na and K) is far too slow to affect the lifetime. We investigate how this shorter atmospheric lifetime impacts the use of SF_6 to derive stratospheric age-of-air. The age-of-air derived from this shorter lifetime SF_6 tracer is longer by 9% in polar latitudes at 20 km compared to a passive SF_6 tracer. We also present laboratory measurements of the infrared spectrum of SF_6 and find good agreement with previous studies. We calculate the resulting radiative forcings and efficiencies to be, on average, very similar to those reported previously. Our values for the 20, 100 and 500-year global warming potentials are 18,000, 23,800 and 31,300, respectively.

1 Introduction

Sulphur hexafluoride (SF_6) is an anthropogenic greenhouse gas which is mainly used as an electrical insulator, with other applications as a quasi-inert gas. Although its main sources are in the Northern Hemisphere, its atmospheric abundance is increasing globally in response to these emissions and its long atmospheric lifetime (defined as the ratio of the atmospheric burden of a trace gas to its rate of loss from the atmosphere). SF_6 is characterised by large absorption cross-sections for terrestrial infrared radiation such that the presently increasing SF_6 abundance will contribute a positive radiative forcing over many centuries. The important known removal sources are electron attachment and photolysis. Recently, Totterdill *et al.*, (2015) have also measured bimolecular rate constants for the reaction of SF_6 with mesospheric metals.

Harnisch and Eisenhauer (1998) reported that SF_6 is naturally present in fluorites, and out-gassing from these materials leads to a natural background atmospheric abundance of 0.01 pptv. However, at present the anthropogenic emissions of SF_6 exceed the natural ones by a factor of 1000 or more and are responsible for the rapid increase in its atmospheric abundance. Surface measurements show that atmospheric SF_6 has increased steadily since the 1980s (Geller *et al.*, 1997; Maiss and Brenninkmeijer, 1998) and is still increasing fairly linearly. The current global mean surface mixing ratio is 8.60 pptv, which increasing by about 0.33 pptv/year (~4%/yr) (Dlugokencky et al., 2016).

SF_6 provides a useful tracer of atmospheric transport in both the troposphere and stratosphere. Rates for transport of pollutants into, within, and out of the stratosphere are important parameters that regulate stratospheric composition. The basic characteristics of the stratospheric Brewer-Dobson (B-D) circulation are known from observations of trace gases such as SF_6: air enters the stratosphere at the tropical tropopause, rises at tropical latitudes, and descends at middle and high latitudes to return to the troposphere. Understanding the rate of this transport on a global scale is crucial in order to predict the response of stratospheric ozone to climatic or chemical change. SF_6 is essentially inert in the troposphere to middle stratosphere and is removed by electron attachment and photolysis in the upper stratosphere and mesosphere (Ravishankara *et al.*, 1993). This tracer therefore provides an ideal probe of transport on timescales of importance in the stratospheric circulation and quantitative information on mean air mass age for the lower and middle stratosphere.

The mean age-of-air (AoA) is the interval between the time when the volume mixing ratio of

a linearly increasing atmospheric tracer reaches a certain value at a given location in the stratosphere and an earlier time when this mixing ratio was reached at a reference location. Mean AoA is expressed as (Hall and Plumb, 1994; Waugh and Hall, 2002)

$$\mathrm{AoA} = t(\chi, l, z) - t(\chi, l_0, z_0) \quad \text{(E1)}$$

where t is time, χ is the volume mixing ratio, l and z are latitude and altitude, and the 0 subscripts denote the reference latitude and altitude which are chosen to be the upper tropical troposphere (for the purposes of our simulations we chose the gridpoint latitude = 1^{o}N, altitude = 13.9 km). In principle the trend of AoA can be used to diagnose changes in the strength of Brewer-Dobson circulation (BDC); in practice, however, it is very difficult to obtain unambiguous results on trends from this or any other trace gas (Garcia *et al.*, 2011). Ideally, AoA should be determined experimentally using a tracer with very small (or zero) chemical sink in the stratosphere or mesosphere. Otherwise, a correction must be applied to account for this loss. A correction would also be necessary for any non-linear tropospheric growth. However, for the period considered for diagnosing age-of-air in this paper (2002-2007) the growth of SF_6 is approximately linear, so we can reasonably neglect such a correction for SF_6-derived AoA (Hall and Plumb, 1994).

Ravishankara *et al.* (1993) reported the atmospheric lifetime of SF_6 to be 3200 years by considering electron attachment and vacuum ultraviolet (VUV) photolysis. They also studied the loss of SF_6 by reaction with $O(^1D)$ but found the rate too slow to be important. They deduced that electron attachment was the dominant loss process and quantified this process using a 2-D model, wherein they assumed that all SF_6 molecules are destroyed after attachment of an electron (with a rate constant of 10^{-9} cm^3 $molecule^{-1}$ s^{-1}). They therefore argued that their lifetime of 3200 years could be a lower limit, but clearly this result depends on the accuracy of the 2-D electron density, which was calculated using only photochemistry. Morris *et al.* (1995) subsequently extended the work of Ravishankara *et al.* (1993) by including an ion chemistry module in the same 2-D model. They also made other assumptions to maximise the impact of electron attachment on SF_6 loss and derived a lifetime as low as 800 years (which could be further sporadically decreased by large solar proton events). Using a 3-D middle atmosphere model, Reddmann *et al.* (2001) estimated the lifetime to be 472 years when SF_6 is irreversibly destroyed purely by direct electron attachment and to be 9379 years when SF_6 loss is assumed to occur only via indirect loss (via the formation of SF_6^-) and ionization via the reactions with O_2^+ and N_2^+. They concluded that the estimated lifetime depends strongly on the electron

attachment mechanism, because the efficiency of this process as a permanent removal process of SF_6 depends on the competition between reaction of SF_6^- with H and HCl, and photodetachment and reaction with O and O_3. Here we extend on the above studies and investigate the SF_6 lifetime using a state-of-the-art 3-D chemistry climate model with a domain from the surface to 140 km. Our modelled electron density is based on results of a detailed ion chemistry model and we use a detailed methodology for treating the atmospheric background electrons, which is based on Troe's formalism (Troe *et al.*, 2007a,b; Viggiano *et al.*, 2007).

In addition to determining the SF_6 lifetime, in this study we report new measurements of the infrared absorption cross-sections for SF_6 and input these into a line-by-line radiative transfer model in order to obtain radiative forcings and efficiencies. These values are then used to determine more accurate values of global warming potentials (GWPs) based on their cloudy sky adjusted radiative efficiencies. GWP is the metric used by the World Meteorological Organisation (WMO) and Intergovernmental Panel on Climate Change (IPCC) to compare the potency of a greenhouse gas relative to an equivalent emission of CO_2 over a set time period. The definitions of these radiative terms are given in Appendix A.

2 Methodology

2.1 WACCM 3D model

To simulate atmospheric SF_6 we have used the Whole Atmosphere Community Climate Model (WACCM). Here we use WACCM 4 (Marsh *et al.*, 2013), which is part of the NCAR Community Earth System Model (CESM; Lamarque *et al.*, 2012), configured to have 88 pressure levels from the surface to the lower thermosphere (5.96×10^{-6} Pa, 140 km) and a horizontal resolution of $1.9^o \times 2.5^o$ (latitude × longitude). The model contains a detailed treatment of middle atmosphere chemistry including interactive treatments of Na and K (Plane *et al.*, 2015). We use the specified dynamics (SD) version of the model to allow comparison with observations (see Garcia *et al.*, (2014) for details). The SF_6 surface emission flux and initial global vertical profiles were taken from a CCMI (Chemistry Climate Model Initiative) simulation using the same version of SD-WACCM with the same nudging analyses (D. Kinnison, personal communication, 2013).

Lyman-α photolysis is the only SF_6 loss reaction in the standard version of WACCM and in this work we have added the additional processes given in **Table 1**. The rate constants for the SF_6 + metal reactions have been measured in our laboratory for mesospheric conditions (Totterdill *et al.*, 2015); here we use the experimental values for the reactions with Na and K.

For the photolysis of SF_6 we used the standard WACCM methodology but with the updated Lyman-α cross section from our laboratory of 1.37×10^{-18} cm^2 $molecule^{-1}$ (Totterdill *et al.*, 2015). The WACCM Lyman-α flux is taken from Chabrillat and Kockarts (1997).

Electron attachment to SF_6 plays a major role in its atmospheric removal and so both dissociative and non-dissociative attachment are considered in this study. The detailed method is described in a recent paper (Totterdill *et al.*, 2015) and here only a brief summary is given. The removal process by the attachment of low energy electrons to SF_6 can be described using Troe's theory (Troe *et al.*, 2007a,b; Viggiano *et al.*, 2007). In the middle and lower mesosphere, electrons are mostly attached to neutral species in the form of anions. However, above 80 km the concentration of free electrons increases and the direct electron attachment to SF_6 becomes more likely. This can happen either by associative attachment forming the SF_6^- anion which can then undergo chemical reactions with H, O, O_3 and HCl, or by dissociative attachment forming the SF_5^- anion fragment. The probability β of dissociative attachment when an electron is captured by SF_6 is given by

$$\beta(p,T) = \frac{k_{dis}}{k_{at}+k_{dis}} \quad \text{(E2)}$$

where k_{dis} is the rate constant for dissociative attachment and k_{at} is the rate constant for associative attachment. β can be expressed as

$$\beta(p,T) = exp(-4587T + 7.74) \times 10^{\left[4.362-0.582log_{10}(p/Torr)-0.0203\left(log_{10}\left(\frac{p}{Torr}\right)\right)^2/5.26\times10^{-4}\right]} \quad \text{(E3)}$$

where T is the temperature in K and p is the pressure in Torr (Totterdill *et al.*, 2015).

We include both associative and dissociative electron attachment using WACCM-predicted electron concentrations (see **Table 1**). Note that the SF_6^- anion is not modelled directly. As it is short-lived we can treat it as being in steady-state and consider the relative rates of its destruction pathways. Therefore, the net SF_6 attachment loss rate is calculated by multiplying k_{at} by the ratio of of permanent destruction of the resulting SF_6^- (reactions of SF_6^- with H and HCl) to the total sum of these reactions plus processes which recycle SF_6^- to SF_6 (reactions with O and O_3, and photodetachment).

In order to use a realistic electron concentration, the role of negative ions in the *D* region must be considered. The *D* region is the lowest part of the ionosphere, extending from about 60 to 85 km. It is characterized by the appearance of cluster ions (e.g. proton hydrates $H^+.(H_2O)_n$, where $n \leq 6$) and negative ions (e.g. O_2^-, CO_3^- and NO_3^-) rather than free electrons. These species predominate because the atmospheric pressure is high enough to facilitate the three-body attachment of ligand species like H_2O to positive ions, and electrons to neutral molecules. Therefore, a scaling factor was introduced that converts the standard WACCM electron concentrations, which are calculated from charge balance with the five major positive *E* region ions (N^+, N_2^+, O^+, O_2^+ and NO^+), to more realistic electron concentrations. We have recently incorporated the Sodankylä Ion Chemistry (SIC) model into the standard version of WACCM to produce a new version (WACCM-SIC) containing a detailed *D* region ion chemistry with cluster ions and negative ions (Kovács *et al.*, 2016). The mesospheric positive and negative ions in WACCM-SIC are listed in **Table 2**. The electron scaling factor in each grid box of WACCM was then defined as the annually averaged ratio of $[e]_{WACCM\text{-}SIC}/[e]_{WACCM}$ for the year 2013, where $[e]_{WACCM\text{-}SIC}$ is the electron density calculated from WACCM-SIC and $[e]_{WACCM}$ from the standard WACCM.

The scaling factor, which varies with altitude and latitude, is shown in **Figure 1** (bottom panel) together with the electron densities from the standard WACCM (top panel) and WACCM-SIC (middle panel) models. The annually averaged electron concentration in the WACCM-SIC model is significantly smaller in the lower and middle mesosphere than in the standard WACCM, which is expected because of negative ion formation. In the polar regions the scaling factor is around 0.01 at 50 km and 0.5 at 70km. Note that in the upper mesosphere (70 - 80 km) the electron density in WACCM-SIC is larger than WACCM, by over a factor 5 near the poles. This results from the inclusion of medium energy electrons (MEE) (electrons with energy between 30 keV and 2 MeV) in WACCM-SIC. **Figure 2** shows the effect of MEE by comparing WACCM-SIC runs with and without this source of ionization in the upper mesosphere included. To describe the effect of ionization, WACCM-SIC uses ionization rates (*I*) as a function of time and pressure which were calculated from the spectra based on the proton energy-range measurements in standard air as described by Verronen *et al.* (2005). According to Figure 3 of Meredith *et al.* (2015), the annually averaged medium energy electron flux for 2013 approximately corresponds to the long-term, 20-year average. This allows us to assume that the annually averaged electron density of 2013 from WACCM-SIC can be used to

scale the long-term simulations using the standard WACCM aimed at determining the atmospheric lifetime of SF_6.

The WACCM simulation included five different SF_6 tracers in order to quantify the importance of different loss processes. All of these tracers used the same emissions but differed in their treatment of SF_6 loss reactions. One SF_6 tracer included no atmospheric loss (i.e. a passive tracer). Three tracers included one of the following loss processes for SF_6: (i) reaction with mesospheric metals (Na, K), (ii) electron attachment, and (iii) UV photolysis. Finally, one 'total reactive' SF_6 tracer included all three loss processes. This total reactive tracer should be the most realistic and was used in the radiative forcing calculations. WACCM was run for the period 1990-2007, and the first five years were treated as spin-up. For the analysis the monthly mean model outputs were saved and later globally averaged for the lifetime calculations.

2.2 Infrared absorption spectrum and radiative forcing

Previous quantitative infrared absorption spectra of SF_6 have been compared in Hodnebrog *et al.* (2013) (their Table 12). There are differences of ~10% between existing integrated cross-section estimates, and the measurements cover different spectral ranges. We therefore performed a more complete set of measurements over a wider spectral range, in order to reduce uncertainty in the absorption spectrum and hence the radiative efficiency of SF_6. Measurements were taken using an experimental configuration consisting of a Bruker Fourier transform spectrometer (Model IFS/ 66), which was fitted with a mid-infrared (MIR) source used to generate radiation which passed through an evacuable gas cell with optical path length 15.9 cm. The cell was fitted with KBr windows, which allow excellent transmission between 400 and 40,000 cm^{-1}. The choice of source and window were selected so as to admit radiation across the mid IR range where bands of interest are known to occur. Room temperature (296 ± 2 K) measurements were carried out between 400 and 2000 cm^{-1} at a spectral resolution of 0.1 cm^{-1} and compiled from the averaged total of 128 scans to 32 background scans at a scanner velocity of 1.6 kHz. Gas mixtures were made using between 8 and 675 Torr of SF_6 diluted up to an atmosphere using N_2, according to the method described in Totterdill *et al.* (2016).

Radiative forcing calculations were made using the Reference Forward Model (RFM) (Dudhia, 2013) which is a line-by-line radiative transfer model based on the previous GENLN2 model (Edwards, 1987). Results obtained from this model were validated against the DISORT

radiative transfer solver (Stamnes *et al.*, 2000) included within the libRadtran (Library for Radiative Transfer) package (Mayer and Kylling, 2005). A full description of these models and parameters used alongside discussion of treatment of clouds and model comparison is also given in Totterdill *et al.* (2016).

3 Results

3.1 Global distributions of SF6 from WACCM simulations

Figure 3 shows typical zonal mean profiles of the WACCM SF_6 tracers in the north and south polar regions for different seasons, compared to MIPAS observations for the year 2007 (Haenel *et al.*, 2015). Although the MIPAS SF_6 data provides much more coverage horizontally and vertically compared to in situ aircraft and balloon data, it has only been validated up to 35 km (Stiller *et al.*, 2008). Validation at higher altitudes is not possible due to the lack of suitable reference data. Details of the validation of the MIPAS data version used here (V5h_SF6_20 for the full resolution product from 2004 and earlier; V5r_SF6_222 and V5r_SF6_223 for the reduced resolution period of 2005 and later) can be found in Haenel *et al.* (2015), including Figure S-2 of their supplementary material. The WACCM passive SF_6 tracer has a mixing ratio profile that is almost constant with altitude in the stratosphere and lower mesosphere below 60 km, then decreases by about 10% by 70 km, after which it decreases more rapidly. Comparison of the tracers that include loss processes show that removal of SF_6 is dominated by electron attachment, with a small contribution (<3%) direct from photolysis. The mesospheric metals make a negligible contribution because the Na and K layers occur in the upper mesosphere above 80 km (with peaks around 90 km), and the concentrations of these metal atoms are too low. **Figure 3** shows that the model mean profile agrees well with the MIPAS mean in the polar lower stratosphere (around 20 km) but exhibits a positive bias of around 1 pptv at higher altitudes in the middle stratosphere. However, the figure also shows that the variability in the observed SF_6 at high latitides is large. The time variation of modelled SF_6 shown in **Figure 4** corresponds to an emission rate (slope) of 6.5×10^{-3} Tg/year, i.e. a 0.29 pptv/year increase in global mean volume mixing ratio, and a volume mixing ratio of 6.4 pptv by the end of 2007.

Figure 5 shows the zonal mean annual mean SF_6 distribution from the five WACCM tracers and MIPAS observations for 2007. **Figure 5a** (and **Figure 3**) shows that there is a rapid decrease in SF_6 above 75 km even for the inert tracer. This can be explained by diffusive separation, which becomes pronounced in the upper mesosphere because SF_6 is a relatively heavy molecule (molar mass 0.146 kg) compared to the mean mass of air molecules (mean

molar mass 0.0288 kg) (cf. Garcia *et al*. (2014), where similar behaviour is seen for CO_2, another relatively heavy molecule). Panels (a)-(c) of the figure all show SF_6 decreasing above ~80 km, and panels (a) and (c) are almost identical, while in panel (b) the decrease begins about 4 km lower. This is all consistent with the notion that metals do not affect SF_6 and photolysis contributes only slightly. The fact that diffusive separation prevents SF_6 from reaching altitudes where photolysis is faster must be contributing to the very long lifetime (48,000 years, **Table 3**) found when photolysis is the only loss considered. By contrast, in **Figure 5d** SF_6 decreases rapidly above 70 km, which is related to the fact that loss via electron attachment is important at these lower altitudes. Thus, in this case, SF_6 loss occurs below the altitudes (~90 km) where diffusive separation is important (and where air density is higher), which makes it a much more effective loss mechanism. The WACCM SF_6 tracer that includes all loss processes (**Figure 5e**) has a very similar distribution to that which only treats loss due to electron attachment (**Figure 5d**), which emphasises how this process dominates SF_6 loss in the model. This model tracer can be compared to the MIPAS observations in **Figure 5f**, which shows that WACCM appears to reproduce the general features of the MIPAS distribution (note the smaller altitude range in panels (e) and (f) of **Figure 5**). However, it is also clear that WACCM SF_6, even with all losses considered, decreases with altitude much more slowly at all latitudes than MIPAS SF_6. This could indicate a problem with the model's meridional transport. However, a too-fast BDC would tend to produce low levels of SF_6 at middle and high latitudes in the descending branch, which does not seem to be the case. Therefore, at least two other possible scenarios could be responsible for the discrepancy: SF_6 loss in WACCM is still somewhat underestimated despite the inclusion of the electron attachment, or MIPAS SF_6 is biased low above ~20 km.

3.2 Atmospheric lifetime

The atmospheric lifetime is defined as the ratio of the atmospheric burden to the atmospheric loss rate. This definition was used to calculate annual mean lifetime values from the WACCM output containing the individual rates for the different loss processes. During the simulation the total atmospheric burden of SF_6 increased linearly as expected (see **Figure 4**) from 3.4×10^{32} molecules with an annual increment of 2.3×10^{31} molecules/year. **Figure 6** shows the variation in SF_6 lifetime from 1995 to 2007, corresponding to a full solar cycle (the solar minima occurred in May 1996 and January 2008). The figure demonstrates that the lifetime has a strong dependence on solar activity, being anti-correlated with solar activity, for example as measured by the radio flux at 10.7 cm (2800 MHz) (Tapping, 2013) which ranges over $(72 – 183) \times10^{-22}$ W m^{-2} Hz^{-1}, with an average value of 90.3×10^{-22} W m^{-2} Hz^{-1}. The mean SF_6 lifetime over the

same solar cycle period is 1278 years, with a range from 1120 to 1475 years. The annual averaged electron number density in the polar regions is also plotted in **Figure 6**; as expected, it is correlated with the 10.7 cm radio emission (Tapping, 2013).

As noted in Section 1, the SF_6 lifetime has been reported to be 3200 years by Ravishankara *et al.*, (1993). For this they used a total electron attachment rate constant of $k_{EA} = 10^{-9}$ cm^3 s^{-1}. In Morris *et al.* (1995) the calculated lifetime decreased to 800 years by considering ion chemistry and assuming that the associative attachment forming SF_6^- does not regenerate the parent molecule, thereby obtaining a lower limit for the lifetime. Reddmann *et al.* (2001) estimated the lifetime to be 472 years when SF_6 is irreversibly destroyed purely by direct electron attachment and to be 9379 years when SF_6 loss is assumed to occur only via indirect loss (via the formation of SF_6^-) and ionization via the reactions with O_2^+ and N_2^+. In the present study we have directly applied Troe's theory (Troe *et al.*, 2007a,b; Viggiano *et al.*, 2007) to determine the efficiency of electron attachment as a function of temperature and pressure, and the branching ratio for dissociative attachment (equation E2), which we extrapolated to mesospheric conditions (Totterdill *et al.*, 2015).

Our estimated *partial* lifetime of SF_6 due to photolysis (i.e. the lifetime calculated considering photolysis as the only atmospheric loss process) for the SF_6 tracer which includes all loss processes is 48,000 yr, which is considerably longer than that the 13,000 yr determined by Ravishankara *et al.* (1993) despite our Lyman-α cross section (1.37×10^{-18} cm^2, **Table 1**) being only ~22% smaller than the value the value measured by Ravishankara *et al.* (1.76×10^{-18} cm^2). One reason why our photolysis-related partial lifetime is longer is that WACCM includes diffusive separation, which was not described in the earlier 2-D model study. The inclusion of diffusive separation reduces sharply the abundance of SF_6 at high altitudes, where photolysis is most effective. Another contributing factor could be that the VUV photolysis is important only above 80 km, while in our model runs SF_6 is mostly destroyed by electron attachment, which results in less being transported into this upper mesospheric region. When we analyse our WACCM SF_6 tracer which is subject to photolysis loss only, the resulting steady-state *overall* lifetime (i.e. lifetime calculated using the rates of all loss processes) for the last model year (2007) is 17,200 yr which is only 32% larger than the value of Ravishankara *et al.* (1993) and thus more consistent with the difference in the Lyman–α cross sections. Finally, if we do not include the electron scaling factor to reduce the electron density below 80 km due to

negative ion formation, then the SF_6 lifetime decreases to 776 years (not shown), which is similar to the value of 800 years obtained by Morris *et al*. (1995).

3.3 Impact of SF_6 loss on mean age of stratospheric air

As SF_6 is a chemically stable molecule in the stratosphere and troposphere, and has an almost linearly increasing tropospheric abundance, its atmospheric mixing ratio is often used to determine the mean age of stratospheric air. This is an important metric in atmospheric science as the distribution of ozone and other greenhouse gases depends significantly on the transport of air into, within, and out of the stratosphere. WACCM contains an idealized, linearly-increasing age-of-air tracer (AOA1) that provides model age values for model experiments (Garcia *et al.*, 2011).

Age-of-air has generally been derived from observations by treating SF_6 as a passive (non-reactive) tracer. The assumption is that the global loss rate is too slow to significantly affect the lifetime. This was confirmed by Garcia *et al.* (2011) when only photolysis was included. However, when loss via electron attachment is also considered, the lifetime may become short enough that this assumption is no longer valid, in which case the stratospheric mixing ratio would appear to correspond to an earlier tropospheric mixing ratio than in reality. We have compared the passive WACCM SF_6 tracer with that subject to all loss processes, which yields the new lifetime of 1278 yr. The difference between these two tracers indicates the error in the derived age-of-air that would arise in the real atmosphere if SF_6 is assumed to be a passive tracer. The error caused by chemical removal can be expressed as:

$$\Delta(\text{AoA}) = \text{AoA(reactive tracer)} - \text{AoA(passive tracer)} \quad \text{(E4)}$$

where Δ(AoA) is the difference in the age-of-air value caused by chemical loss, AoA(reactive tracer) is the calculated age-of-air considering the chemical removal, and AoA(passive tracer) is the value obtained from a non-reactive tracer. The expression for the age-of-air at any point in the stratosphere can be obtained from a simplified version of (E1) that is derived from a Taylor series expansion, retaining only the linear term. It is then expressed as

$$\text{AoA} = [(\chi_0(SF_6) - \chi(SF_6))/\, r(SF_6)] \quad \text{(E5)}$$

where $\chi(SF_6)$ and $\chi_0(SF_6)$ are the SF_6 volume mixing ratios at the actual and the reference (tropical tropopause) points, respectively, while $r(SF_6)$ is the rate of increase of tropospheric SF_6. In our simulations $r(SF_6)$ is 0.29 pptv/year (**Figure 4**), which is an approximation as the

growth rate is not constant in reality. Stiller *et al.* (2012) report a value of 0.24 pptv/year based on observations over the MIPAS period. These two simplifications will lead to deviations between WACCM and MIPAS age data. If (E5) is substituted into (E4) then the error in age-of-air will be:

$$\Delta(\mathrm{AoA}) = (\chi(\mathrm{SF_{6,\ passive}}) - \chi(\mathrm{SF_{6,\ reactive}}))/\ r(\mathrm{SF_6}) \qquad \text{(E6)}$$

This error, along with the mean age itself, was calculated from WACCM output for 2007. **Figure 7** shows the annual mean ages determined from the WACCM simulation from 2002-2007 using the total reactive and the inert SF_6 tracers and the idealized AOA1 age tracer. There is a clear difference between the age values derived from the passive SF_6 and the idealized AoA tracer. If equation (E5) is used to determine the age values there is no guarantee that the age values derived from the two tracers will be identical; the rate was determined from the increase of the SF_6 burden (0.29 pptv/year) and this was provided by the linear fit (**Figure 4**), which can misrepresent the growth rate at a specific time. **Figure 7** also shows the difference between the age values obtained from the reactive and inert SF_6 tracers. It can be seen that consideration of the reactive SF_6 tracer does indeed affect the determined mean age values, mostly where electron attachment dominates. The age estimates at high latitudes are most sensitive to chemical loss because the air that reaches these locations has descended from the high altitudes where SF_6 loss predominantly occurs. According to the MIPAS satellite observations (Stiller *et al.*, 2012; Haenel *et al.*, 2015.), the derived age value over the tropical lower stratosphere at 25 km is slightly more than 3 years, while the WACCM simulations with the reactive SF_6 tracer predicts 3 years. Comparing **Figures 7a** and **7b**, the effect of chemical removal in this region is minor (0.01 year or 0.5% change) and therefore it does not have much impact on the inferred atmospheric transport. At the poles the effect is much more significant; the difference at 25 km between the reactive and inert SF_6 tracers is up to 0.55 years (9%). In summary, in the troposphere-stratosphere at low latitudes the effect of chemical removal is not very significant and the error on the estimated mean age caused by the assumption of SF_6 being a passive tracer is not important. However, the effect of chemical removal becomes more significant at high latitudes.

We can also compare modelled and observed mean age values in the lower stratosphere (20 km). **Figure 8** shows the mean age profiles from WACCM tracers, ER-2 observations (Hall *et al.*, 2009) and our analysis of MIPAS SF_6 satellite data at 20 km. From this it can be seen that in the tropical region the mean age values are similar between the idealized age tracer and the

inert and reactive SF_6 tracers. This is consistent with no loss of SF_6 having occurred in air parcels in the deep tropics. At high latitudes there is up to 0.5 year difference in the modelled mean ages, with the reactive SF_6 tracer producing the oldest apparent age. The differences in mean age between the tracers is larger in the SH polar region than in the NH because the polar region is less well mixed. The tendency is very similar when we compare the WACCM mean ages to the MIPAS observations. Note that the satellite observations show more seasonal variability in the middle and high latitudes than in the tropics.

3.4 Radiative Efficiency and Forcing

To determine the radiative efficiency and global warming potential of SF_6, integrated cross-sections were taken from two public Molecular Spectroscopic Databases: (i) the GEISA-2009/2011 Spectroscopic Database (Jacquinet-Husson *et al*., 2011), which uses the data of Varanasi (2001) and Hurley (2003), and (ii) the HITRAN-2012 Molecular Spectroscopic Database (Rothman *et al*., 2012) which uses the data of the Pacific Northwest National Laboratory Infra-Red Database (Sharpe *et al*., 2004). Values were also measured in this study. The literature values are presented in **Table 4** for comparison with our experimentally determined values and the full SF_6 spectrum obtained in this study is given in **Figure 9**. In our study the spectrometer error is ±1.0% for all experiments, and the uncertainty in the sample concentrations of SF_6 was calculated to be 0.7%. Spectral noise was averaged at $\pm 5\times10^{-21}$ cm^2 molecule^{-1} per 1 cm^{-1} band. However, at wavenumbers <550 cm^{-1}, towards the edge of the mid infrared where opacity of the KBr optics increases, this value was 1×10^{-20} cm^2 molecule^{-1} per 1 cm^{-1} band. The error from determining the scaling cross-section was 5%. This results in an average overall error of ±5% in the cross-sections.

The intensities of the main SF_6 absorption bands (925-955 cm^{-1}) measured in this study are 7% greater than those reported by Hurley (2003), 1% greater than Varanasi (2001) and 1% lower than those given in HITRAN (Rothman *et al.*, 2012) (**Table 4**). Comparison of our results against Varanasi (2001) between 650 and 2000 cm^{-1} gives an agreement within 9%. Note that these differences are within the combined error of both experiments.

The instantaneous and stratospheric adjusted SF_6 radiative efficiencies in clear and cloudy sky conditions are given in **Table 5**. These are also presented as present-day radiative forcings employing a current surface concentration of 9.3 pptv (NOAA, 2016) (see **Figure 4**). The radiative efficiency was calculated in the RFM for each month between 90ºS and 90ºN at latitudinal resolutions (on which the data was averaged to obtain the zonal mean vertical

profile) of 1.5° and 9.0°. The tropopause used the standard WMO lapse rate definition (see Totterdill *et al.*, 2016). **Figure 10** shows the seasonal-latitudinal variation of the instantaneous clear sky radiative forcing for SF_6 on the high (1.5°) and low (9°) resolution grids. Employing profiles averaged over the lower resolution grid gives an average forcing within 1% of the higher resolution grid. Using only a single annually averaged global mean profile led to a 10% error in radiative forcing when compared to our monthly resolved high resolution profile, supporting the findings of Freckleton *et al.* (1998) and Totterdill *et al.* (2016).

A selection of experiments were carried out over a range of months and latitudes to investigate the sensitivity of the forcing calculations to the bands used. The average contributions from the main bands were compared against the calculation with the full measured spectrum. The results showed that the 580 – 640 and 925 – 955 cm^{-1} bands contribute almost 99% to the instantaneous radiative forcing. Our forcing calculations suggest that the SF_6 minor bands contribute only a small amount to the final value. This means that deviations between our experimentally determined spectra and those in the literature only result in a significant change to previously published radiative forcings and efficiencies when that deviation occurs over a major band.

The SF_6 adjusted cloudy sky radiative efficiency published by the IPCC AR5 report and used to determine its GWP values is 0.57 Wm^{-2} $ppbv^{-1}$ (Myhre *et al.*, 2013). This compares to our adjusted cloudy sky radiative efficiency of 0.59 Wm^{-2} $ppbv^{-1}$ (Table 5). A review on radiative efficiencies and global warming potentials by Hodnebrog *et al.* (2013) provides a comprehensive list of all published values for these parameters for many species including SF_6. They established the range of published radiative efficiencies for SF_6 to be 0.49 – 0.68 Wm^{-2} $ppbv^{-1}$, with a mean value of 0.56 Wm^{-2} $ppbv^{-1}$. They also made their own revised estimate using an average of the HITRAN (Rothman *et al.*, 2012) and GEISA (Jacquinet-Husson et al., 2011) spectral databases and found a best estimate of (0.565 ± 0.025) Wm^{-2} $ppbv^{-1}$. Their mean value for radiative efficiency is very close to that determined in this study using similar conditions (0.59 Wm^{-2} $ppbv^{-1}$).

3.5 Global Warming Potential

Table 6 gives our estimates of the 20, 100 and 500-year GWPs based on cloudy sky adjusted radiative efficiencies of SF_6 compared with IPCC AR5 values (IPCC, 2013). Our 20, 100 and 500-year global warming potentials for SF_6 are 18,000, 23,800 and 31,300 respectively. The 20-year and 100-year values are 3% greater and 1% greater, respectively, than their IPCC counterparts and the 500-year GWP is 4% smaller than its AR4 counterpart (Forster *et al.*,

2007). The forcing efficiencies determined in this study are somewhat higher than the previously published values (see Section 3.4), which would imply a higher GWP value. However, our shorter atmospheric lifetimes would lead to a smaller GWP estimate, with a larger effect at longer time horizons when atmospheric loss becomes relevant. The trade-off between these competing effects is apparent in **Table 6**, where SF_6 exhibits a 20-year GWP that is slightly larger than the IPCC value, while the 500-year GWP is slightly smaller. The radiative efficiency effect is most obvious for the case of the 20-year GWP where, because the atmospheric lifetime of SF_6 is 1278 years, the species does not have time for any significant loss to occur.

4 Conclusions

The 3D Whole Atmosphere Community Climate Model was used to simulate the SF_6 atmospheric distribution over the period of 1995-2007. From the concentrations and the knowledge of the electron attachment, photolysis and metal reaction rates we determined the atmospheric lifetime which shows a significant dependence (-12% to +15%) on the solar cycle due to varying electron density. The mean SF_6 atmospheric lifetime and 1σ variation over a solar cycle were determined to be 1278 years (ranging from 1120 to 1475 years), which is different to previously reported literature values and much shorter than the widely quoted value of 3200 years. The reason is our more detailed treatment of electron attachment using a new formalism to describe both associative and dissociative attachment, and the use of a detailed model of *D* region ion chemistry to evaluate the partitioning of electrons and negative ions below 80 km. Further refinement to this lifetime estimate from modelling studies depends on decadal length simulations of the model with detailed ion chemistry for the realistic long-term estimation of electron density in the upper atmosphere without the need for scaling factors as employed here.

Based on this new estimate of the SF_6 lifetime, we find that the derived mean age of stratospheric air from observations can be slightly affected by the atmospheric removal of SF_6. In the polar region the age-of-air values differ by up to 9% when the values from inert and reactive model tracers are compared, suggesting that SF_6 loss does not have a large influence on the age values but that it should be included in detailed analyses.

We also re-investigated the radiative efficiency and global warming potential of SF_6. Our radiative efficiency value reported here, 0.59 ± 0.045 Wm^{-2} $ppbv^{-1}$, is slightly higher than the IPCC AR5 estimate of 0.57 Wm^{-2} $ppbv^{-1}$. The global warming potentials of SF_6 for 20, 100

and 500 years have been determined to be 18,000, 23,800 and 31,300, respectively. We find that our revised lifetime and efficiency values somewhat cancel each other out so overall do not play a significant role in modifying the GWP estimates on these time horizons.

Acknowledgements

This work was part of the MAPLE project funded by research grant NE/J008621/1 from the UK Natural Environment Research Council, which also provided a studentship for AT. The authors are also thankful to Prof Jürgen Troe for the helpful discussions related to the electron attachment to SF_6. MPC was supported by a Royal Society Wolfson Merit Award. Simulations were performed on the Archer and University of Leeds HPC systems.

Appendix A

The climate metrics used in this paper are defined in the following ways.

- Radiative forcing (RF) is the change in the net irradiance at the tropopause after allowing stratospheric temperatures to adjust to radiative equilibrium (expressed in watts per square metre; Wm^{-2}) due to an internal or external change in the forcing of the climate system, such as a change in the concentration of CO_2 or the output of the Sun.
- Radiative efficiency is the radiative forcing per kg of compound.
- Global warming potential (GWP) is defined by the expression:

$$GWP = \frac{\int_0^{TH} a_\chi[\chi(t)]dt}{\int_0^{TH} a_r[r(t)]dt} \quad \text{(E6)}$$

where TH is time horizon; a_χ is radiative forcing due to a unit increase in atmospheric abundance of the compound (Wm^{-2} kg^{-1}) and [χ(t)] is its time-dependent decay in concentration following its instantaneous release at time t=0. The denominator contains the corresponding quantities for CO_2 as a reference gas (Myhre *et al.*, 2013). GWP is the most common metric used by the WMO and IPCC to compare the potency of a greenhouse gas relative to an equivalent emission of CO_2 over a set time period. GWP takes into account species lifetime. This means a species with a very high radiative forcing may still have a low GWP if it also possesses a short atmospheric lifetime. However, GWP does not account for factors such as changes in emission or the introduction of replacement species. Criticisms of GWP are discussed in greater detail by Myhre et al. (2013).

References

Chabrillat, S. and Kockarts, G.: Simple parameterization of the absorption of the solar Lyman-alpha line, Geophys. Res. Lett., 24, 2659-2662, 1997.

Dlugokencky, E.J., B.D. Hall, M.J. Crotwell, S.A. Montzka, G. Dutton, J.Mühle and J.W. Elkins: Long-lived greenhouse gases [in "State of the Climate in 2015"], Bull. Amer. Meteor. Soc., 97 (8), S44-S46, 2016.

Dudhia, A.: Reference Forward Model V4.30: http://www.atm.ox.ac.uk/RFM, 2013.

Edwards, D. P.: GENLN2: The new Oxford line-by-line atmospheric transmission/radiance model, Clarendon Laboratory, Oxford, 1987.

Freckleton, R. S., Highwood, E. J., Shine, K. P., Wild, O., Law, K. S., and Sanderson, M. G.: Greenhouse gas radiative forcing: Effects of averaging and inhomogeneities in trace gas distribution, Q. J. Roy. Meteor. Soc., 124, 2099-2127, 10.1002/qj.49712455014, 1998.

Forster, P., V. Ramaswamy, P. Artaxo, T. Berntsen, R. Betts, D.W. Fahey, J. Haywood, J. Lean, D.C. Lowe, G. Myhre, J. Nganga, R. Prinn, G. Raga, M. Schulz and R. Van Dorland: Changes in Atmospheric Constituents and in Radiative Forcing. *In: Climate Change 2007: The Physical Science Basis. Contribution of Working Group I to the Fourth Assessment Report of the Intergovernmental Panel on Climate Change,* Cambridge University Press, Cambridge, United Kingdom and New York, NY, USA, 2007.

Garcia, R. R., Randel, W. J., and Kinnison, D. E.: On the determination of age of air trends from atmospheric trace species, J. Atmos. Sci., 68, 139-154, 2011.

Garcia, R. R., López-Puertas, M., Funke, B., Marsh, D. R., Kinnison, D. E., Smith, A. K. and González-Galindo, F.: On the distribution of CO_2 and CO in the mesosphere and lower thermosphere, J. Geophys. Res., 119, 5700-5718, 2014.

Geller, L. S., Elkins, J. W., Lobert, J. M., Clarke, A. D., Hurst, D. F., Butler, J. H., and Myers, R. C.: Tropospheric SF_6: Observed latitudinal distribution and trends, derived emissions and interhemispheric exchange time, Geophys. Res. Lett., 24, 675-678, 1997.

Haenel, F.J., Stiller, G.P., von Clarmann, T., Funke, B., Eckert, E., Glatthor, N., Grabowski, U., Kellmann, S., Kiefer, M., Linden, A. and Reddmann, T.: Reassessment of MIPAS age of air trends and variability, Atmos. Chem. Phys., 15, 13161-13176, 2015.

Hall, T.M., and Plumb, R.A.: Age as a diagnostic of stratospheric transport. J. Geophys. Res., 99, 1059-1070, 1994.

Hall, T. M., Waugh, D. W., Boering, K. A., and Plumb, R. A.: Evaluation of transport in stratosphere models, J. Geophys. Res., 104, 18815-18839, 1999.

Harnisch, J., and Eisenhauer, A.: Natural CF_4 and SF_6 on Earth, Geophys. Res. Lett., 25, 2401-2404, 1998.

Hodnebrog, Ø., Etminan, M., Fuglestvedt, J. S., Marston, G., Myhre, G., Nielsen, C. J., Shine, K. P., and Wallington, T. J.: Global warming potentials and radiative efficiencies of halocarbons and related compounds: A comprehensive review, Rev. Geophys., 51, 300-378, 10.1002/rog.20013, 2013.

Hurley, M. D.: GEISA : 2011 Spectroscopic Database; SF_6 Infrared Absorption Cross-sections, 2003.

IPCC: Climate Change 2013: The Physical Science Basis. Contribution of Working Group I to the Fifth Assessment Report of the Intergovernmental Panel on Climate Change, Cambridge University Press, Cambridge, United Kingdom and New York, NY, USA, 1535 pp., 2013.

Jacquinet-Husson, N., Crepeau, L., Armante, R., Boutammine, C., Chédin, A., Scott, N.A., Crevoisier, C., Capelle, V., Boone, C., Poulet-Crovisier, N., Barbe, A., Campargue, A., Chris Benner, D., Benilan, Y., Bézard, B., Boudon, V., Brown, L.R., Coudert, L.H., Coustenis, A., Dana, V., Devi, V.M., Fally, S., Fayt, A., Flaud, J.-M, Goldman, A., Herman, M., Harris, G.J., Jacquemart, D., Jolly, A., Kleiner, I., Kleinböhl, A., Kwabia-Tchana, F., Lavrentieva, N., Lacome, N., Li-Hong, Xu, Lyulin, O.M., Mandin, J.-Y, Maki, A., Mikhailenko, S., Miller, C.E., Mishina, T., Moazzen-Ahmadi, N., H.S.P. Müller, A. Nikitin, J. Orphal, V. Perevalov,Perrin, D.T. Petkie, A. Predoi-Cross, Rinsland, C.P., Remedios,J.J., Rotger, M., Smith, M.A.H., Sung, K., Tashkun, S., Tennyson, J., Toth, R.A., Vandaele, A.-C., J. Vander Auwera, J.: The 2009 edition of the GEISA spectroscopic database. J. Quant. Spectrosc. Radiat. Transfer, 112, 2395–2445, 2011.

Kovács, T., Plane, J. M.C., Feng, W., Nagy, Chipperfield, M. P., Verronen, P. T., Andersson, M. E., Newnham, D. A., Clilverd, M. A., and Marsh, D. R.: *D*-region ion–neutral coupled chemistry (Sodankylä Ion Chemistry, SIC) within the Whole Atmosphere Community Climate Model (WACCM 4) – WACCM-SIC and WACCM-rSIC, Geosci.Model Dev., 9, 3123-3136, doi:10.5194/gmd-9-3123-2016, 2016.

Lamarque, J.-F., Emmons, L. K., Hess, P. G., Kinnison, D. E., Tilmes, S., Vitt, F., Heald, C. L., Holland, E. A., Lauritzen, P. H., Neu, J., Orlando, J. J., Rasch, P., and Tyndall, G.: CAM-chem: description and evaulation of interactive atmospheric chemistry in CESM., Geosci. Model Dev., 5, 369-411, 2012.

565 Maiss, M., and Brenninkmeijer, C. A. M.: Atmospheric SF_6, trends, sources and prospects.,
566 Environ. Sci. Technol., 32, 3077-3086, 1998.

567 Marsh, D. R., Mills, M. J., Kinnison, D. E., and Lamarque, J.-F.: Climate change from 1850 to
568 2005 simulated in CESM1 (WACCM), J. Climate, 26, 7372-7391, 2013.

569 Mayer, and Kylling: Technical note: The libRadtran software package for radiative transfer
570 calculations - description and examples of use, Atmos. Chem. Phys., 5, 1855-1877, 2005.

571 Meredith, N. P., Horne, R. B., Isles, J. D., and Rodriguez, J. V.: Extreme relativistic electron
572 fluxes at geosynchronous orbit: Analysis of GOES E > 2 MeV electrons, Space Weather,
573 13, 170-184, 2015.

574 Morris, R. A., Miller, T. M., Viggiano, A. A., Paulson, J. F., Solomon, S., and Reid, G.: Effects
575 of electron and ion reactions on atmospheric lifetimes of fully fluorinated compounds, J.
576 Geophys. Res., 100, 1287-1294, 1995.

577 Myhre, G., Shindell, D., Bréon, F.-M., Collins, W., Fuglestvedt, J., Huang, J., Koch, D.,
578 Lamarque, J.-F., Lee, D., Mendoza, B., Nakajima, T., Robock, A., Stephens, G., Takemura,
579 T., and Zhang, H.: Anthropogenic and natural radiative forcing, Cambridge (UK), New
580 York (USA), 2013.

581 NOAA Earth System Research Laboratory, Halocarbons and other atmospheric trace gases,
582 SF_6 – Combined Dataset, http://www.esrl.noaa.gov/gmd/hats/combined/SF6.html,
583 [Accessed 1/1/2016], 2016.

584 Plane, J. M. C., Feng, W., and Dawkins, E. C. M.: The mesosphere and metals, Chem. Rev.,
585 115, 4497-4541, 2015.

586 Ravishankara, A. R., Solomon, S., Turnipseed, A. A., and Warren, R. F.: Atmospheric lifetimes
587 of long-lived haloganated species, Science, 259, 194-199, 1993.

588 Reddmann, T., Ruhnke, R., and W. Kouker,W.: Three-dimensional model simulations of SF_6
589 with mesospheric chemistry, J. Geophys. Res., 106, 14,525–14,537,
590 doi:10.1029/2000JD900700, 2001.

591 Rothman, L. S., Gordon, I. E., Babikov, Y., Barbe, A., Benner, D. C., Bernath, P. F., Birk, M.,
592 Bizzocchi, L., Boudon, V., Brown, L. R., Campargue, A., Chance, K., Cohen, E. A.,
593 Coudert, L. H., Devi, V. M., Drouin, B. J., Faytl, A., Flaud, J. M., Gamache, R. R., Harrison,
594 J. J., Hartmann, J. M., Hill, C., Hodges, J. T., Jacquemart, D., Jolly, A., Lamouroux, J., Roy,
595 R. J. L., Li, G., Long, D. A., Lyulin, O. M., Mackie, C. J., Massie, S. T., Mikhailenko, S.,
596 Müller, H. S. P., Naumenko, O. V., Nikitin, A. V., Orphal, J., Perevalov, V., Perrin, A.,

Polovtseva, E. R., Richard, C., Smith, M. A. H., Starikova, E., Sung, K., Tashkun, S., Tennyson, J., Toon, G. C., Tyuterev, W. G., and Wagner, G.: The HITRAN 2012 Molecular Spectroscopic Database, J. Quant. Spectrosc. Radiat. Transfer, 4 - 50, 2012.

Sharpe, S.W., Johnson, T.J., Sams, R.L., Chu, P.M., Rhoderick, J.C.: Gas-Phase Databases for Quantitative Infrared Spectroscopy, Appl Spectrosc., 58(12), 1452-1461, 2004.

Stamnes, K., Tsay, S. C., Wiscombe, W., and Laszlo, I.: DISORT, a General-Purpose Fortran Program for Discrete-Ordinate-Method Radiative Transfer in Scattering and Emitting Layered Media: Documentation of Methodology, 2000.

Stiller, G. P., von Clarmann, T., Höpfner, M., Glatthor, N., Grabowski, U., Kellmann, S., Kleinert, A., Linden, A., Milz, M., Reddmann, T., Steck, T., Fischer, H., Funke, B., Lopez-Puertas, M., and Engel, A.: Global distribution of mean age of stratospheric air from MIPAS SF_6 measurements, Atmos Chem Phys, 8, 677–695, 2008.

Stiller, G. P., von Clarmann, T., Haenel, F., Funke, B., Glatthor, N., Grabowski, U., Kellmann, S., Kiefer, M. Linden, A., Lossow, S. and López-Puertas, M.: Observed temporal evolution of global mean age of stratospheric air for the 2002 to 2010 period, Atmos. Chem. Phys., 12, 3311-3331, 2012.

Tapping, K. E.: The 10.7 cm solar radio flux (F10.7), Space Weather, 11, 394-406, 2013.

Totterdill, A., Kovács, T., Gomez-Martin, J. C., Feng, W., and Plane, J. M. C.: Mesospheric removal of very long-lived greenhouse gases SF_6 and CFC-115 by metal reactions, Lyman-α photolysis, and electron attachment, J. Phys. Chem. A, 115, 2016-2025, 2015.

Totterdill, A., Kovács, T., Feng, W., Dhormse, S., Smith, C., Martin, J. C. G., Chipperfield, M., Forster, P., and Plane, J.: Atmospheric Lifetimes, Infrared Absorption Spectra, Radiative Forcings and Global Warming Potentials of NF_3 and CFC-115, Atmos. Chem. Phys., 16, 11,451-11,463, doi:10.5194/acp-2016-231, 2016.

Troe, J., Miller, T. M., and Viggiano, A. A.: Low-energy Electron Attachment to SF_6. I. Kinetic modeling of nondissociative attachment, J. Chem. Phys., 127, 244303, 2007a.

Troe, J., Miller, T. M., and Viggiano, A. A.: Low-energy electron attachment to SF_6. II. Temperature and pressure dependences of dissociative attachment, J. Chem. Phys., 127, 244304, 2007b.

Varanasi, P. SF_6 Infrared Absorption Cross-Sections. 2001 [Accessed 03/03/2015] Available from: http://ether.ipsl.jussieu.fr/ether/pubipsl/GEISA/geisa_crossIR_frame_2011_uk.jsp.

628 Verronen, P. T., Seppälä, A., Clilverd, M. A., Rodger, C. J., Kyrölä, E., Enell, C.-F., Ulich, T.,
629 and Turunen, E.: Diurnal variation of ozone depletion during the October-November 2003
630 solar proton events, J. Geophys. Res., 110, A09S32, 2005.
631 Viggiano, A. A., Miller, T. M., Friedman, J. F., and Troe, J.: Low-energy electron attachment
632 to SF_6. III. From thermal detachment to the electron affinity of SF_6, J. Chem. Phys., 127,
633 244305, 2007.
634 Waugh, D., and Hall, T: Age of stratospheric air: Theory, observations and models, Rev
635 Geophys., 40, doi:10.1029/2000RG000101, 2002.
636

637 **Tables**

638 **Table 1**. SF_6 loss reactions included in WACCM.

Loss process	Rate constant	Reference and comments
Na + SF_6	$k = 1.80\times10^{-11}\exp(-590.5/T)$	From Totterdill *et al.*, (2015) Refitted for mesospheric temperatures 215-300K.
K + SF_6	$k = 13.4\times10^{-11}\exp(-860.6/T)$	From Totterdill *et al.*, (2015) Refitted for mesospheric temperatures 215-300K.
Electron attachment	Associative attachment: $k_{EA,ass} = k_{at} \times (k_{(SF6^- + H)}[H] + k_{(SF6^- + HCl)}[HCl]) / (j_{PD} + k_{(SF6^- + H)}[H] + k_{(SF6^- + HCl)}[HCl] + k_{(SF6^- + O3)}[O_3] + k_{(SF6^- + O)}[O])$ Dissociative attachment: $k_{EA,diss} = k_{at} \times \beta$, where β is the fraction of SF_6^- that dissociates into SF_5^-.	Totterdill *et al.*, (2015).
Photolysis	Lyman-α: $\sigma(121.6\ nm) = 1.37\times10^{-18}\ cm^2$ Parameterised expression over the range of 115-180 nm, based on previous measurements.	Totterdill *et al.*, (2015).

639

640 **Table 2.** Positive and negative ions included in WACCM-SIC.

Positive ions	O_2^+, O_4^+, NO^+, $NO^+(H_2O)$, $O_2^+(H_2O)$,$H^+(H_2O)$, $H^+(H_2O)_2$, $H^+(H_2O)_3$, $H^+(H_2O)_4$, $H^+(H_2O)_5$, $H^+(H_2O)_6$, $H_3O^+(H_2O)_2(CO_2)$, $H_3O^+(OH)$, $O_2^+(CO_2)$, $H_3O^+(OH)(CO_2)$, $H_3O^+(OH)(H_2O)$, $O_2^+(H_2O)(CO_2)$, $O_2^+(H_2O)_2$, $O_2^+(N_2)$, $NO^+(H_2O)_2$, $H^+(H_2O)(CO_2)$, O^+, N^+, N_2^+, $NO^+(H_2O)_3$, O_4^+, $H^+(H_2O)_2(CO_2)$, $H^+(H_2O)_2(N_2)$
Negative ions	O_3^-, O^-, O_2^-, OH^-, $O_2^-(H_2O)$, $O_2^-(H_2O)_2$, O_4^-, CO_3^-, $CO_3^-(H_2O)$, CO_4^-, HCO_3^-, NO_2^-, NO_3^-, NO_3, (H_2O), $NO_3^-(H_2O)_2$, $NO_3^-(HNO_3)$, $NO_3^-(HNO_3)_2$, Cl^-, ClO^-, $NO_2^-(H_2O)$, $Cl^-(H_2O)$, $Cl^-(CO_2)$, $Cl^-(HCl)$

641

642 **Table 3.** Partial (reactions with electrons, photolysis, and metals (K, Na)) and total atmospheric
643 lifetimes (years) of SF_6 from different studies. Numbers in parentheses show relative
644 percentage contribution of loss due to the different processes.

Study	Lifetime / years			
	Photolysis	Electron attachment	Total	Model dimensions
Ravishankara *et al.* (1993)	13,000 (24%)	4210 (76%)	3200	2D
Morris *et al.* (1995)	N/A	N/A	800	2D
This work	48,000 (2.6%)	1339 (97.4%)	1278	3D

645

Table 4. Integrated absorption cross-sections for SF_6 measured in this work and ratios with values obtained by GEISA (Jacquinet-Husson et al., 2011; Hurley 2003; Varanasi 2001) and HITRAN (Rothman et al., 2012).

		Ratio of integrated cross-sections in this work to previous studies		
Band limits (cm^{-1})	Integrated cross-section (10^{-16} cm^2 $molec^{-1}$ cm^{-1})	Hurley (2003)	Varanasi (2001)	HITRAN
925 - 955	2.02	1.07	1.01	0.99
650 - 2000	2.40	-	1.09	-

Table 5. Calculated instantaneous and stratospheric adjusted radiative forcings and radiative efficiencies of SF_6 in clear and all-sky conditions[a].

	Instantaneous		Stratospheric adjusted	
	Clear	All-sky	Clear	All-sky
Radiative forcing (mWm^{-2})	76.43	48.91	81.81	56.01
Radiative efficiency (Wm^{-2} $ppbv^{-1}$)	0.77	0.50	0.85	0.59

a. Based on present day atmospheric SF_6 surface concentration of 9.3 pptv.

Table 6. Comparison of 20, 100 and 500-year global warming potentials for SF_6 from this work with values from IPCC (2013).

	Global Warming Potential		
	GWP_{20}	GWP_{100}	GWP_{500}
This work[a]	18000	23700	31300
IPCC (2013)[b]	17500	23500	32600[c]
Difference (%) (This work – IPCC)	+3%	+1%	-4%

[a] Based on our atmospheric lifetime of 1278 yrs and RE of 0.59 Wm^{-2} $ppbv^{-1}$.

[b] Based on an atmospheric lifetime of 3200 yrs and RE of 0.57 Wm^{-2} $ppbv^{-1}$.

[c] Based on an atmospheric lifetime of 3200 yrs and RE of 0.52 Wm^{-2} $ppbv^{-1}$ from IPCC AR4 (Forster *et al.*, 2007).

Figures

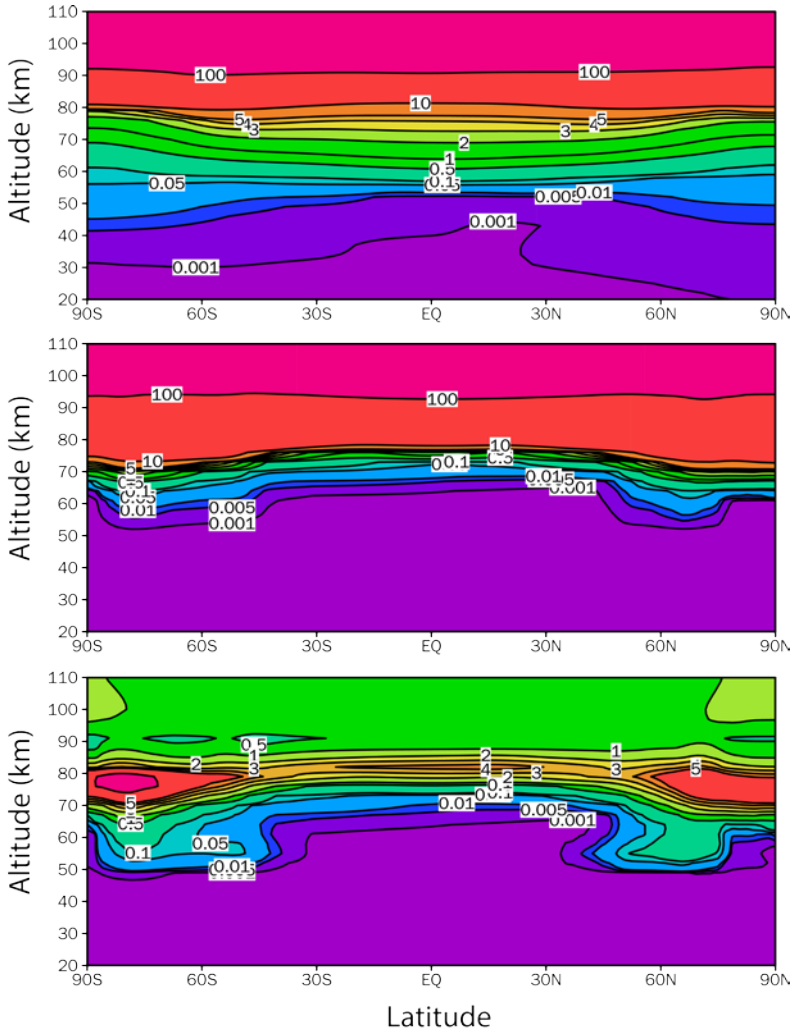

Figure 1. Top: annual average electron concentration for 2013 from the standard WACCM model (in 10^2 electrons cm^{-3}). Middle: annual average electron concentration for 2013 from WACCM-SIC model (in 10^2 electrons cm^{-3}). Bottom: annually averaged electron scaling factor for 2013.

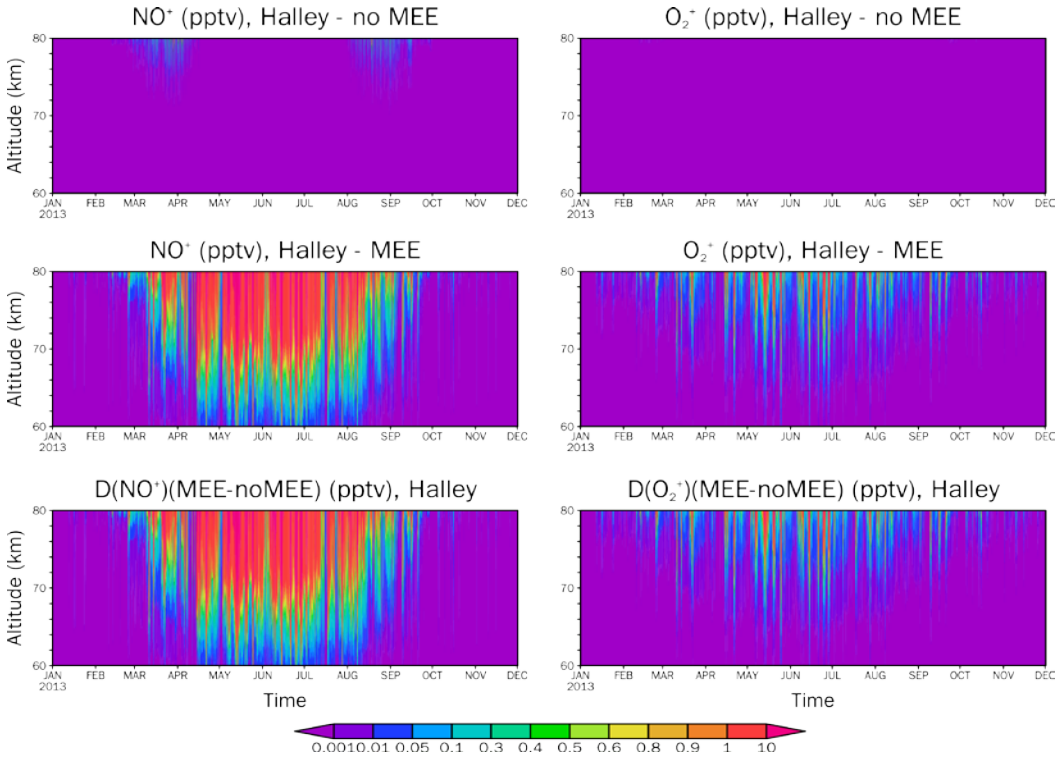

Figure 2. Time series of volume mixing ratio profiles (pptv) of NO^+ (left panels) and O_2^+ (right panels) above Halley (76°S) from two WACCM-SIC simulations. Top panels show the values obtained from the model run without medium energy electrons (MEE); the middle panels show the run with medium energy electrons; and the bottom panels show the absolute differences between the two model runs.

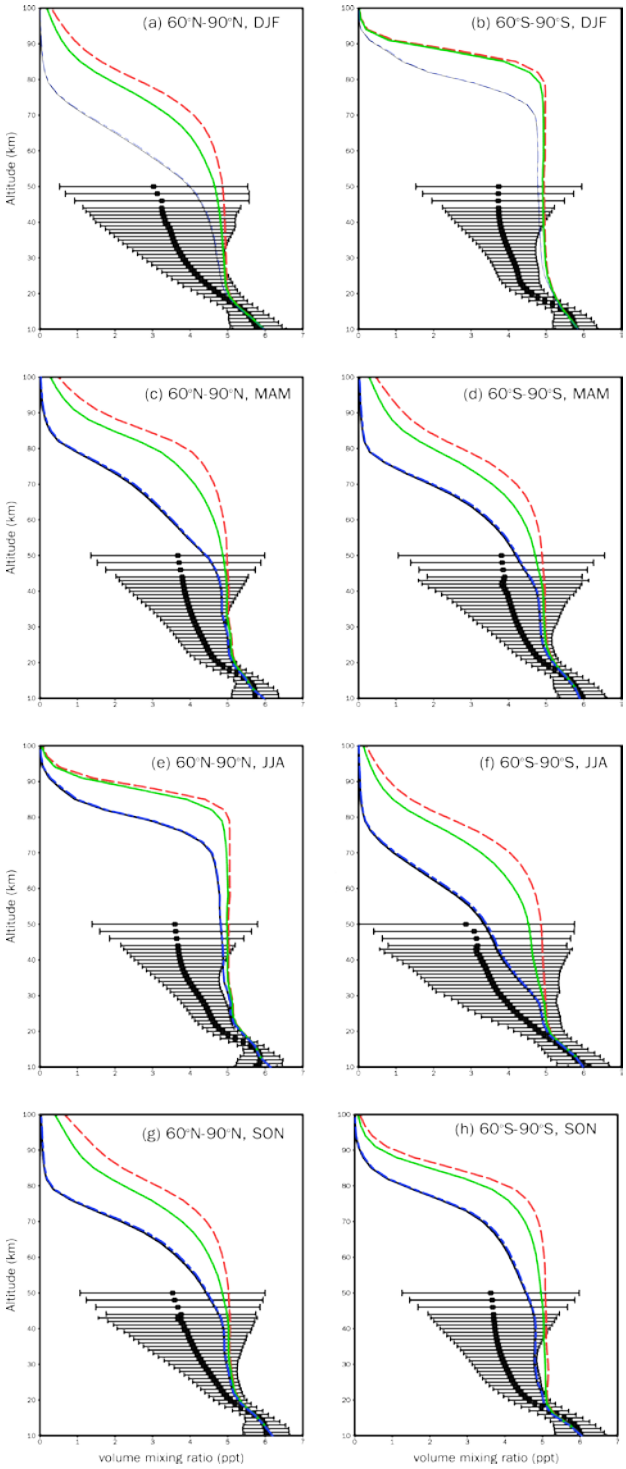

Figure 3. Seasonal mean volume mixing ratios (pptv) of the different SF_6 tracers for the polar regions (60°N – 90°N and 60°S – 90°S latitudes) in 2007 as a function of altitude for MIPAS satellite observed SF_6 (black symbols with standard deviations for ±1σ) (Stiller *et al.*, 2012), the total WACCM-SF_6 (blue solid line), the photolysis WACCM-SF_6 tracer (green solid line) and the inert WACCM SF_6 tracer (red dashed line).

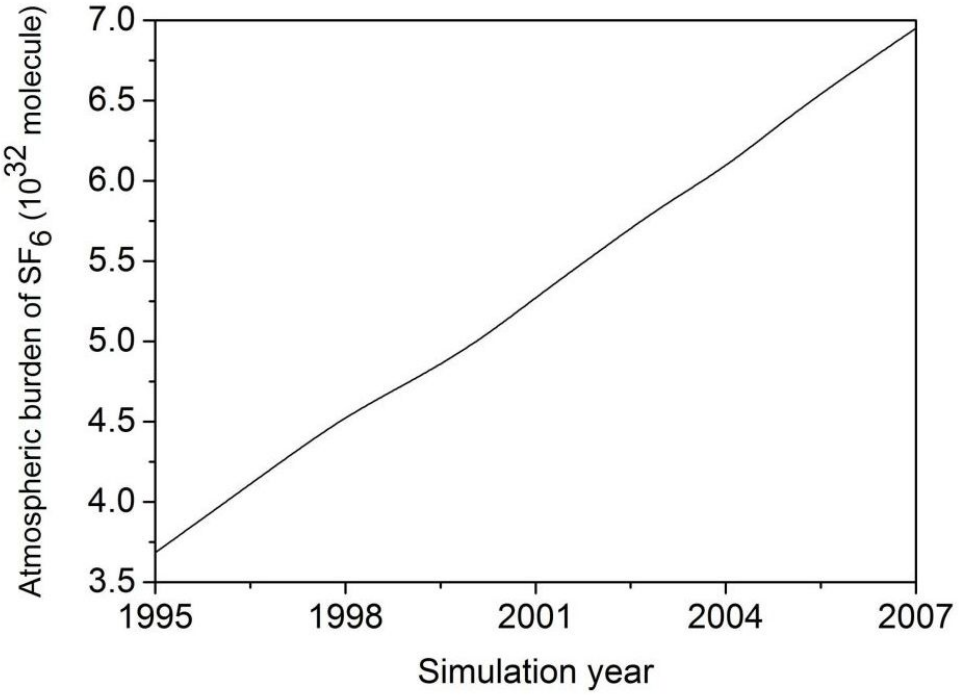

Figure 4. Variation of the total annual atmospheric burden of SF_6 during the simulation from 1995 to 2007. According to this the emission rate (slope) was determined to be 6.5×10^{-3} Tg/year, corresponding to 0.29 pptv/year.

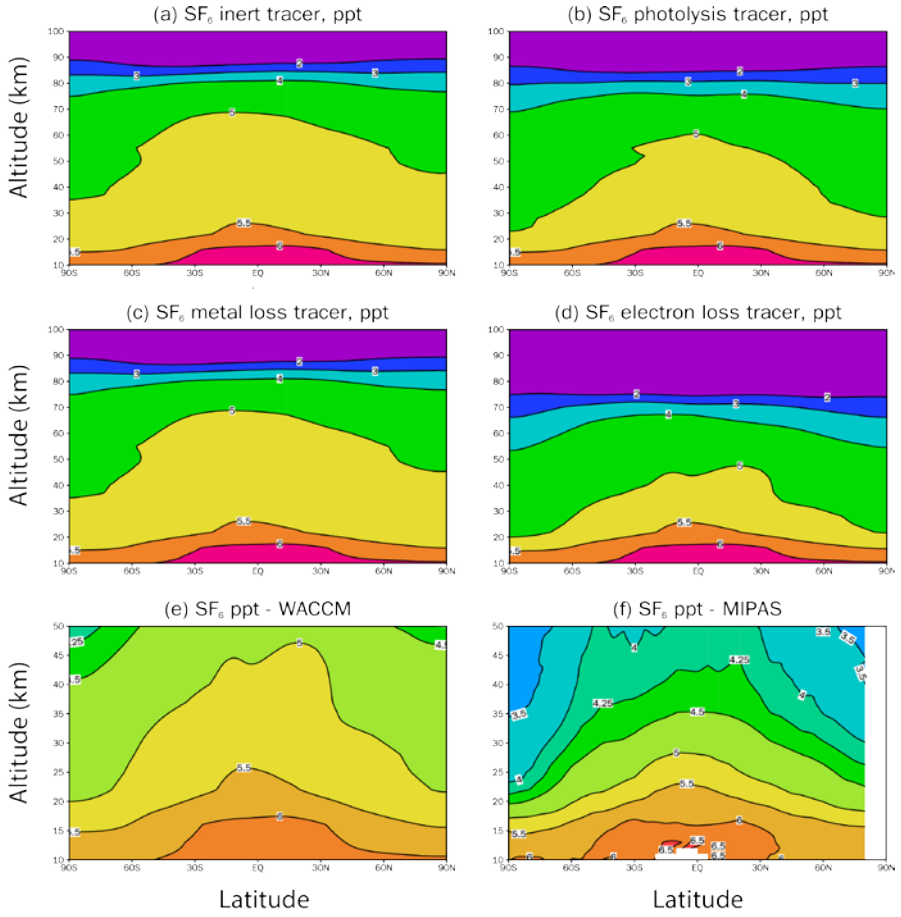

Figure 5. Annual zonal mean latitude-height volume mixing ratios (pptv) of the different WACCM SF_6 tracers in 2007: (a) inert SF_6 tracer; (b) SF_6 tracer removed by photolysis only; (c) SF_6 tracer removed by mesospheric metals only; (d) SF_6 tracer removed by electron attachment only; and (e) total reactive SF_6. Panel (f) shows the SF_6 volume mixing ratio for 2007 from MIPAS observations. Note the different altitude ranges and contour intervals for panels (a)-(d) versus panels (e)-(f).

691

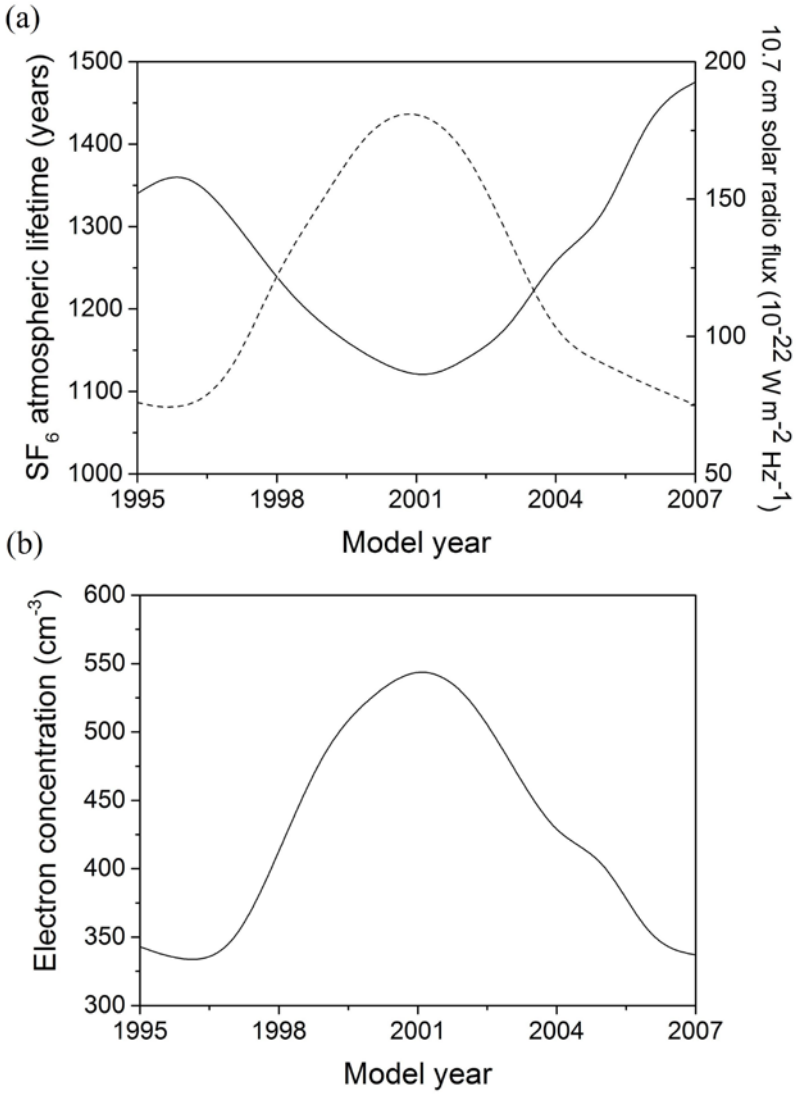

692

693 **Figure 6.** (a) Variation in atmospheric lifetime of SF_6 (solid line) and 10.7 cm solar radio flux
694 (dashed line) during the WACCM simulation. (b) Variation of the WACCM electron
695 concentration (cm^{-3}) at 80 km, averaged over polar latitudes (60°N – 90°N and 60°S – 90°S).

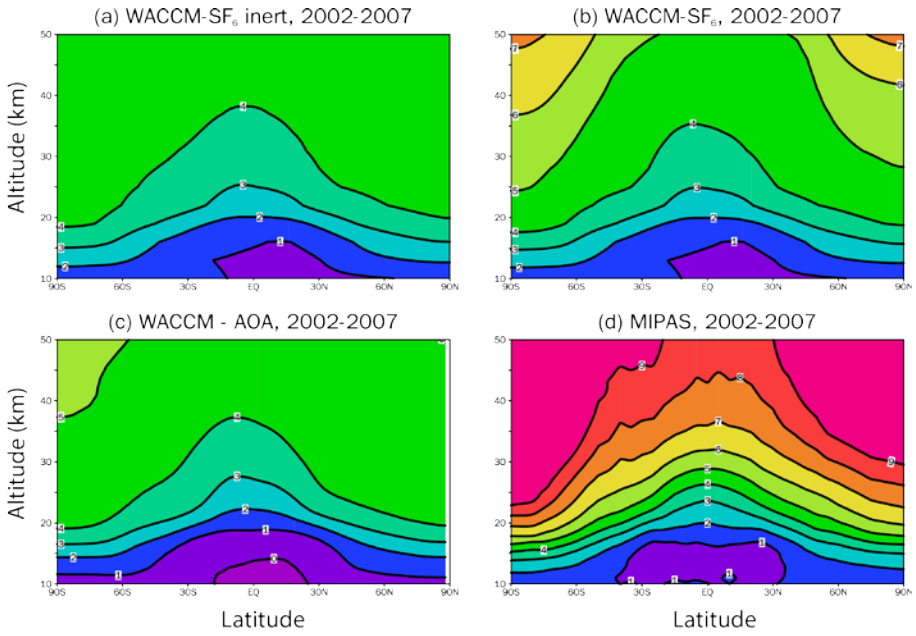

696

697 **Figure 7.** Annual mean age of stratospheric air (years) for the period of 2002–2007 determined
698 from a WACCM simulation using: (a) the inert SF_6 tracer; (b) the total reactive SF_6 tracer; (c)
699 the idealized AOA1 tracer. Panel (d) shows the age values derived for the same period from
700 our analysis of MIPAS SF_6 observations.

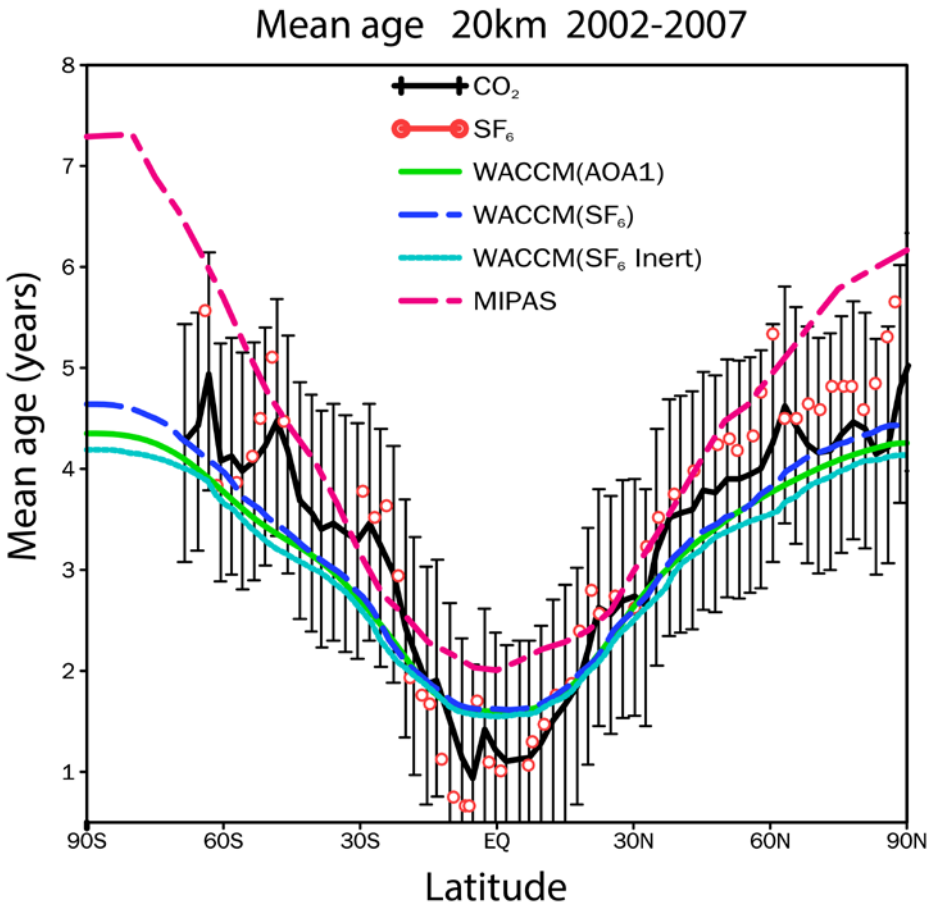

Figure 8. Mean age values at 20 km altitude derived from MIPAS satellite (dashed magenta line) and ER-2 aircraft observations (SF_6 red open circles, CO_2 black crosses) (Hall *et al.*, 1999). The error bars apply to the age derived from the ER-2 observations. Also shown is the mean age derived from WACCM tracers: reactive SF_6 (dashed blue line), passive SF_6 (light blue line) and AOA tracer (solid green line).

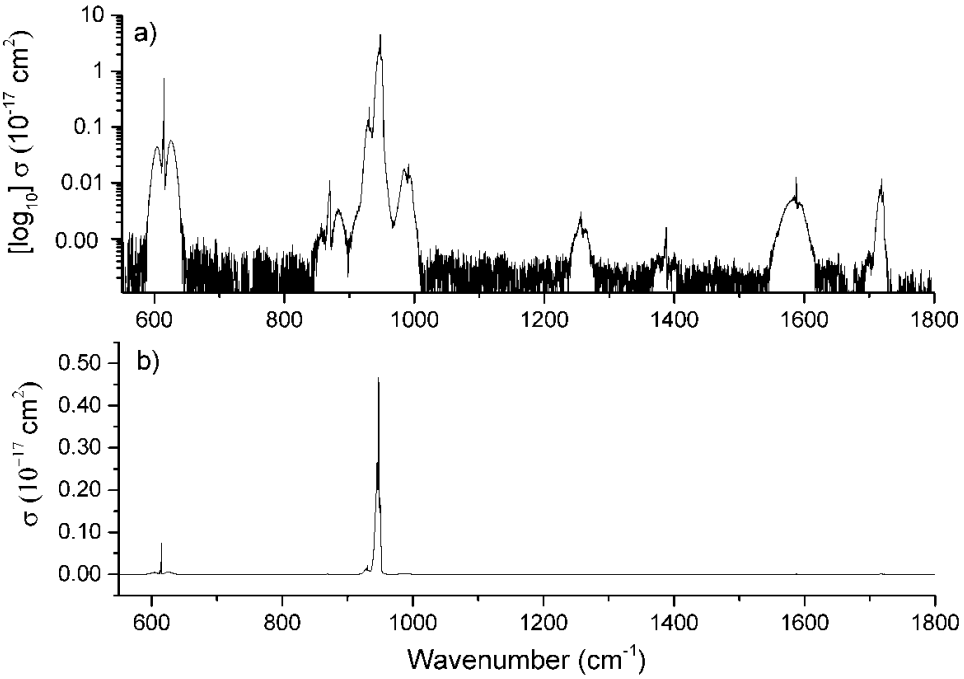

Figure 9. Infrared absorption spectrum of SF_6 at ~295 K on (a) a logarithmic y axis and (b) a linear y axis. The logarithmic scale in panel (a) highlights the relative positions of the minor bands.

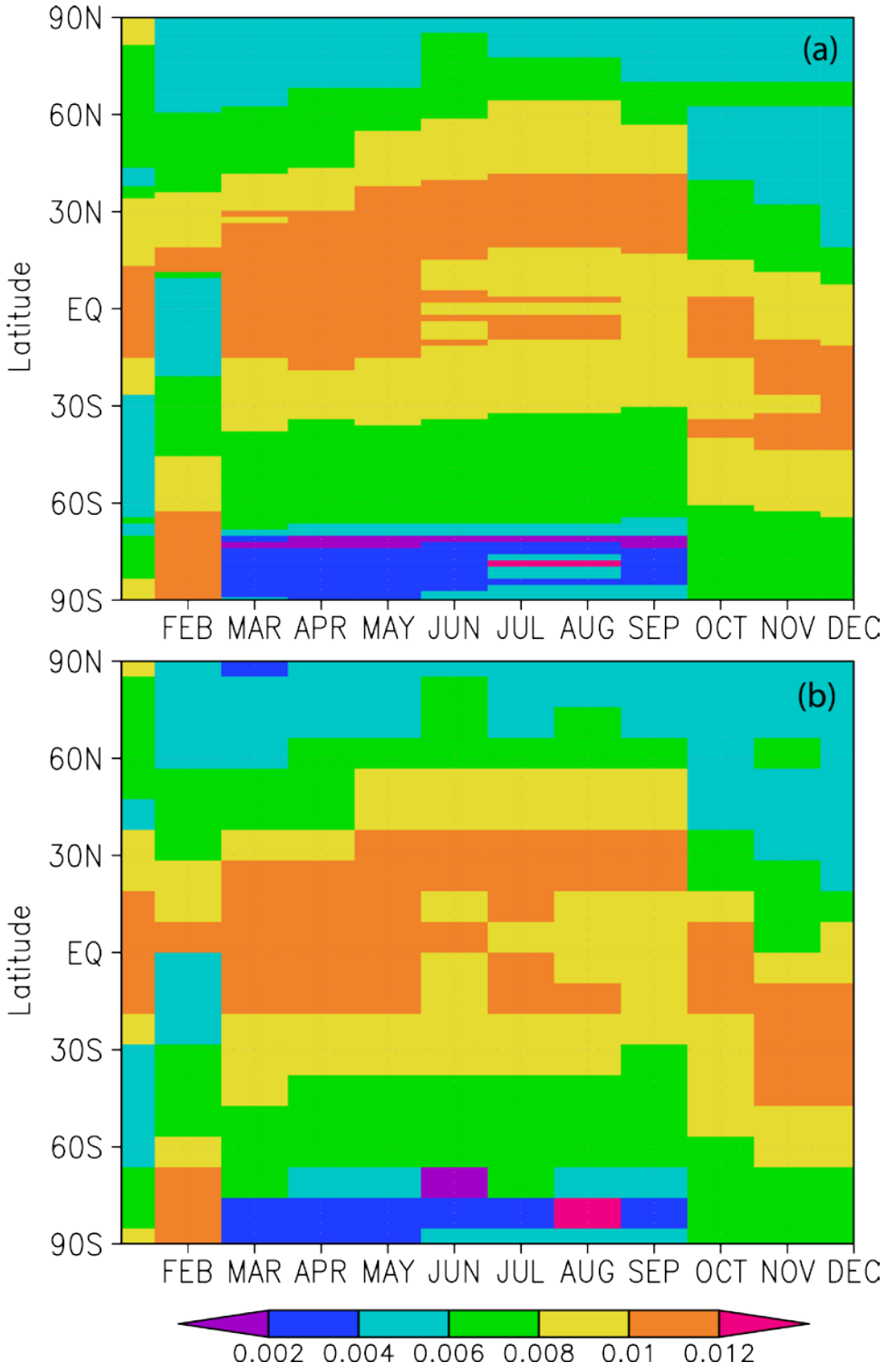

Figure 10. Latitude-time plots for instantaneous radiative forcing (Wm^{-2}) by SF_6 as a function of latitude and month at (a) high latitude resolution (1.5° spacing) and (b) low latitude resolution (9° spacing).